Original Article



# Twelve-week high-fat diet for improving adverse ventricular remodeling post-myocardial infarction by alleviating local inflammation

**Jing Yang[1,2#], Bifang Mai[1,2#], Yinqing Su[1,2,3#], Shumin Liang[1], Zizhuo Su[1,2,4], Yuyang Chen[1,2,4], Shuanglun Xie[1,2,4,5]**

[1]Department of Cardiology, Sun Yat-sen Memorial Hospital of Sun Yat-sen University, Guangzhou, China; [2]Guangdong Province Key Laboratory of Arrhythmia and Electrophysiology, Guangzhou, China; [3]Department of Critical Care Medicine, Guangdong Second Provincial General Hospital, Guangzhou, China; [4]Guangzhou Key Laboratory of Molecular Mechanism and Translation in Major Cardiovascular Disease, Sun Yat-sen Memorial Hospital, Sun Yat-sen University, Guangzhou, China; [5]Guangzhou Key Laboratory of Molecular Mechanism and Translation in Major Cardiovascular Disease, Guangzhou, China

*Contributions:* (I) Conception and design: All authors; (II) Administrative support: Y Chen, S Xie; (III) Provision of study materials or patients: Y Chen, S Xie; (IV) Collection and assembly of data: J Yang, B Mai, Y Su; (V) Data analysis and interpretation: J Yang, B Mai; (VI) Manuscript writing: All authors; (VII) Final approval of manuscript: All authors.

[#]These authors contributed equally to this work.

*Correspondence to:* Shuanglun Xie; Yuyang Chen. Department of Cardiology, Sun Yat-sen Memorial Hospital of Sun Yat-sen University, 107 Yanjiang West Road, Guangzhou 510120, China. Email: xieshlun@mail.sysu.edu.cn; chenyy245@mail.sysu.edu.cn.

**Background:** Many studies have examined how to achieve better outcomes in myocardial infarction (MI) patients with mild obesity or who are overweight. However, the influence of a high-fat diet (HFD) and the underlying mechanisms by which it can affect ventricular remodeling following MI are poorly understood. This study investigated the impact of a 12-week HFD on the left ventricular (LV) remodeling of permanent MI models and immune cell involvement.

**Methods:** Male C57BL/6J mice were fed HFD or normal diet (ND). After 8 weeks of feeding, mice underwent cardiac left anterior descending coronary artery ligation, and the same diet was continued for a further 4 weeks. Cardiac structure and function were detected using echocardiography. Cardiac fibrosis was evaluated using histological staining at 7 and 28 days post-MI. Infiltration of various immune cells was examined using flow cytometry and immunofluorescence at 7 days post-MI.

**Results:** Compared with a ND, the 12-week HFD feeding significantly alleviated ventricular remodeling following MI. HFD mice showed reduced infiltration of neutrophils, a higher proportion of M2/M1 macrophages, decreased conventional and monocyte-derived dendritic cells (moDCs) in the injured myocardium, and elevated levels of regulatory T cells (Tregs). Further investigation of dendritic cells (DCs) phenotypes indicated downregulated expression of major histocompatibility complex class II (MHCII). It also showed costimulatory molecules CD40 and CD86 on conventional and moDCs in mediastinal lymph nodes (mLNs).

**Conclusions:** This study demonstrated the protective effect of a 12-week HFD on ventricular remodeling following MI via the alleviation of local inflammation.

**Keywords:** High-fat diet (HFD); ventricular remodeling; myocardial infarction (MI); inflammation

Submitted Mar 07, 2022. Accepted for publication Jul 04, 2022.
doi: 10.21037/atm-22-1218
**View this article at:** https://dx.doi.org/10.21037/atm-22-1218

## Introduction

Myocardial infarction (MI) is a leading cause of death, especially in developed countries, and remains the prevailing cause of heart failure (HF) worldwide (1). The ischemic heart undergoes cardiomyocyte death, inflammatory infiltration, collagen deposition, and ventricular remodeling, all of which play vital roles in the development of HF (2). Excessive body weight has been defined as a risk for cardiovascular disease (CVD), such as an increased incidence of MI (3). Despite the acknowledged association between obesity and an increased risk of CVD, several studies have found that obesity has a contradictory beneficial effect on the outcome of acute coronary syndromes, a phenomenon called the obesity paradox (4). For example, one study found that, when compared with a healthy weight, there was an inverse association between being overweight or obese with all-cause mortality after acute MI (5). However, whether the obesity paradox is still applicable to acute MI and the potential underlying mechanism are less clear.

Ischemia results in anoxia and nutrient deprivation, leading to cardiomyocyte cell death in the nonperfused territory. This is accompanied by an intense sterile inflammatory response and gradual collagen-driven scar formation required to replace the necrotic myocardium. A growing amount of research supports the finding that inflammation is a driver of ventricular remodeling post-MI. After MI, necrosis of infarcted myocardium triggers an inflammatory immune response, in which multiple innate immune cells participate in clearing up the dead debris. Neutrophils and proinflammatory type1 macrophages (M1) are the main agents that exert this function. The initial proinflammatory phase should be properly resolved by around 4 to 7 days post-MI; it is dominated by anti-inflammatory factors and cells such as type 2 macrophages (M2) from innate immunity and regulatory T cells (Tregs) from adaptive immunity (6). Tregs have a powerful immunosuppressive function that improves cardiac repair by negatively affecting excessive inflammation following MI (7). Furthermore, Tregs suppress inflammation by downregulating costimulatory signals and diminishing the ability of antigen-presenting cells, including dendritic cells (DCs) (8,9).

Although there is a close relationship between obesity and inflammation, the relative research on the impact of the obesity paradox upon inflammation post-MI appears very sparse. Hence, we tested the hypothesis that a high-fat diet (HFD) can improve ventricular remodeling after MI and that the reduction of the inflammatory response mediated by immune cells contributes to the protective effect of a HFD on ventricular remodeling after MI. We present the following article in accordance with the ARRIVE reporting checklist (available at https://atm.amegroups.com/article/view/10.21037/atm-22-1218/rc).

## Methods

### *Mice and feeding*

Experiments were performed under a project license (license no. of laboratory animal facility: SYXK [Guangdong] 2019-0209) granted by the ethics committee of Sun Yat-sen University and in compliance with the Institutional Animal Care and Use Committee (Eighth Edition) for the care and use of animals. Male C56BL/6J mice were purchased from GemPharmatech Co., Ltd. (Nanjing, China) and maintained in the Laboratory Animal Center of Sun Yat-sen University in a certified specific pathogen-free facility (license no. of laboratory animal facility: SYXK [Guangdong] 2019-0209). Mice aged 6 to 8 weeks were fed a HFD (60% of the calories in the HFD were provided by fat; cat. HF60; Dyets Inc., Bethlehem, PA, USA) or a normal diet (ND; ~13% of calories in the ND were provided by fat; cat. GDMLAC-08; Guangdong Medical Laboratory Animal Center, Guangdong, China) for the experiment's duration until they were killed. All mice were housed in a space with no more than 5 mice per cage and maintained on a 12-hour light-dark cycle. Mice had access to autoclaved water and food *ad libitum*. Water and food were added twice a week.

### *Animal experiments*

After 8 weeks of a HFD or a ND feeding, mice were anesthetized with 1.5% sodium pentobarbital (0.1 mL/20 g), intubated, and ventilated with a MiniVent mouse ventilator (Harvard Apparatus, Holliston, MA, USA). MI was induced by permanent ligation of the left anterior descending coronary artery using 9-0 nylon sutures (with a needle; LingQiao, Zhejiang, China). The apex of the heart immediately became pale after ligation. The chest wall and skin were closed with 4-0 nylon sutures (with a needle; Yuanlikang, Jiangsu, China). Animals were put on a heating pad to keep them warm and were ventilated until they woke up. Fifteen mice in the HFD and ND groups underwent cardiac left anterior descending coronary artery ligation.

 

By the end of the experiment, 8 survived in the ND group, representing a survival rate of 53.3%, and 9 survived in HFD group, representing a survival rate of 60%. All the mice died within 7 days of surgery.

### *Echocardiography*

Murine cardiac echocardiography was performed before, 1 week, and 4 weeks after the MI experiment using a Vevo3100 Imaging System (Fujifilm, Tokyo, Japan). A heated, bench-mounted adjustable rail system under 1% to 2% inhaled isoflurane anesthesia was used, with body temperature maintained at 37.0±0.5 ℃ and heart rate at 500±50 bpm. Left ventricular ejection fraction (LVEF), fractional shortening (FS), left ventricular end systolic volume (LVESV), and left ventricular end diastolic volume (LVEDV) were recorded by M-mode tracings in the parasternal long-axis and short-axis views.

### *Isolation of immune cells from the heart*

The whole heart was removed from the mouse. It was first trimmed to remove the connective tissue and aorta on the surface, and then cut into pieces—the thinner, the better. These small pieces were washed with precold phosphate-buffered saline (PBS) until the wash solution was nearly colorless to remove immune cells in the microcirculation system of the myocardial tissue. The pieces from each heart were resuspended with prewarmed 15 mL Roswell Park Memorial Institute (RPMI)-1640 (cat. c11875500bt; Gibco, Thermo Fisher Scientific, Waltham, MA, USA). Added to this was 1 mg/mL of collagenase II (cat. LS004176; Worthington Biochemical Corporation, Lakewood, NJ, USA), 0.02 mg/mL of hyaluronidase (cat. LS002592; Worthington Biochemical Corporation), and 0.02 mg/mL of DNase I (cat. LS002139; Worthington Biochemical Corporation). The resuspension was incubated at 37 ℃ on a shaker at 210 rpm for 60 minutes. After digestion, the digestive sample was immediately put on ice and filtered through a 40-μm cell strainer (cat. 15-1040; Biologix, Jinan, Shangdong). Red blood cells were then lysed by adding 1 mL of ammonium-chloride-potassium (ACK) lysis buffer. After centrifugation, cells were prepared for following flow cytometry staining by resuspending the pellets in 100 μL of PBS.

### *Isolation of immune cells from lymphoid organs (spleen and lymph nodes)*

Lymphoid organs were harvested from mice and transferred in a 40-μm cell strainer placed on top of a 50-mL centrifuge tube. A total of 1–2 mL of PBS was added to the cell strainer. Tissues were carefully ground using the rough end of a 1-mL syringe plunger until only the connective tissue was visible. Cells were pelleted by centrifugation at 400 ×g for 5 minutes at 4 ℃, and the supernatant was aspirated off. A total of 1 mL of ACK lysis buffer was added to each sample to lyse red blood cells, but this step was omitted for lymph nodes. The samples were resuspended by vortexing and incubated at 4 ℃ for 10 minutes. The samples were centrifuged at 400 ×g for 5 minutes at 4 ℃. After the supernatant was aspirated off, cells were diluted appropriately in PBS to obtain a concentration of ~$10^6$/100 μL per sample for subsequent flow cytometric staining.

### *Flow cytometry staining*

Immune cells isolated from the heart or lymphoid organs were added into 1:1,000 anti-ghost-BV510 (cat. 13-0870; Tonbo Biosciences, San Diego, CA, USA) to exclude dead cells and were then incubated on ice for 25 minutes in the dark. PBS (1,000 μL) was added to each sample for washing, and the cells were centrifuged at 400 ×g for 5 minutes at 4 ℃. After the supernatant was aspirated off, the cells were resuspended in 50 μL of stain buffer containing 1:100 anti-CD16/CD32 (cat. 70-0161; Tonbo Biosciences). The samples were resuspended and incubated on ice for 15 minutes in the dark to block nonspecific binding sites. A 50-μL cocktail was added to each sample; the cocktail contained 50 μL of stain buffer and fluorophore-labeled monoclonal antibodies as appropriate for the specific study, CD45 (cat. 147704; BioLegend, San Diego, CA, USA), CD3 (cat. 65-0031; Tonbo Biosciences), CD64 (cat. 139323; BioLegend), CD206 (cat. 61-2061; eBioscience, San Diego, CA, USA), Ly6G (cat. 50-1276; Tonbo Biosciences), CD4 (cat. 35-0042; Tonbo Biosciences), CD11b (cat. 60-0112; Tonbo Biosciences), CD11c (cat. 75-0114; Tonbo Biosciences), major histocompatibility complex class II (MHCII; cat. 35-5321; Tonbo Biosciences), CD40 (cat. 20-8050; Tonbo Biosciences), and CD86 (cat. 64-0862; eBioscience). Samples were incubated on

 

ice for 20 minutes in the dark. The cells were pelleted by centrifugation at 400 ×g for 5 minutes at 4 ℃, and the supernatant was aspirated off. For intracellular or intranuclear staining, a cellular pellet was resuspended with 1 mL of 1× transcription factor fixation/permeabilization working solution (cat. TNB-1020-L050 and TNB-1022-L160; Tonbo Biosciences), and incubated on ice for 60 minutes in the dark and centrifuged at 4,000 ×g for 5 minutes at 4 ℃. Following this, 1 mL of 1× flow cytometry perm buffer working solution (cat. TNB-1213-L150; Tonbo Biosciences) was added and centrifuged at 4,000 ×g for 5 minutes at 4 ℃. After the supernatant was aspirated off, the cells were resuspended in 50 µL of cocktail per sample, which contained 50 µL of 1× flow cytometry perm buffer working solution and fluorophore-labeled monoclonal antibodies against FoxP3 (cat. 50-5773; Tonbo Biosciences). Samples were incubated on ice for 60 minutes in the dark. The cells were pelleted by centrifugation at 4,000 ×g for 5 minutes at 4 ℃, and the supernatant was aspirated off. The cellular pellet was resuspended with 300 µL of PBS, and cell suspension was used for analysis. Data were acquired on a BD flow cytometer (BD Biosciences, Franklin Lake, NJ, USA) and analyzed with FlowJo software version 10.4.

### *Gene expression analyses*

Total RNA from tissues or cells was extracted with TRIzol reagent (cat. 15596026; Invitrogen, Thermo Fisher Scientific, Waltham, MA, USA) following the manufacturer's instructions. Total RNA (1 µg) was reverse-transcribed using PrimerScript reverse transcription (RT) Master Mix (Perfect Real-Time; cat. RR036A; Takara Bio, Kyoto, Japan), and the conditions were 37 ℃ for 15 s and 85 ℃ for 5 s. Quantitative real-time polymerase chain reaction (qRT-PCR) was applied using TB Green Pre-mix Ex Taq (Tli RNaseH Plus) qPCR (cat. RR420A; Takara Bio) on a Bio-Rad CFX Connect system (cat. 185-5096; Bio-Rad, Hercules, CA, USA), and the conditions were 95 ℃ for 10 s followed by 95 ℃ for 5 s and 60 ℃ for 30 s for a total of 40 cycles. Relative messenger RNA (mRNA) levels were normalized to glyceraldehyde 3-phosphate dehydrogenase (GAPDH) using the $2^{-\Delta\Delta CT}$ comparative method. All experiments were performed in triplicate. The qRT-PCR primers used for gene expression are listed in Table S1.

### *Biochemical analysis*

The levels of insulin, triglyceride (TG), total cholesterol (CH), and low-density lipoprotein cholesterol (LDL-C) in the mouse serum were detected using enzyme-linked immunosorbent assay kits. The blood glucose of mice was detected using blood glucose test paper.

### *Immunofluorescence staining*

Mouse hearts were embedded in the optimal cutting temperature (OCT) compound and kept at –20 ℃ after being frozen at –80 ℃. Sections (7-µm thickness) were fixed with 4% paraformaldehyde and labeled with FoxP3 monoclonal antibody (cat. 14-5773-82; eBioscience) at 4 ℃ overnight, followed by a goat anti-rat antibody (cat. A-11081; Invitrogen) for 1 hour at room temperature, and fluoroshield-containing 4,6-diamidino-2-phenylindole (DAPI, cat. F6057; Sigma-Aldrich, St. Louis, MO, USA) was used as the mounting medium. $FoxP3^+$ cells were quantified using confocal microscopy with identical exposure settings at 400-fold magnification.

### *Masson's trichrome staining*

Heart tissues were harvested, embedded, and sectioned in order. The infarction area of the mouse heart, as evidenced by fibrosis that was blue after staining, was examined with a Masson's staining kit (cat. G1340; Solarbio, Beijing, China) according to the manufacturer's protocol. Images were observed with an optical microscope and analyzed with ImageJ software. The percentage of infarction area was equal to the ratio of the area of fibrosis to the total area of the left ventricle.

### *Statistical analysis*

All data were analyzed using GraphPad Prism 9.0 (GraphPad, San Diego, CA, USA) and are expressed as the mean ± standard error of mean (SEM). An unpaired *t*-test with equal or unequal variance was used. P values are indicated with the following symbols: ns, not significant; *P<0.05; **P<0.01; ***P<0.001; and ****P<0.0001.

## Results

### *Twelve-week HFD alleviated ventricular remodeling after MI*

To determine the impact of HFD pretreatment on body weight and systemic metabolism, we fed mice for 8 weeks with ND or HFD and measured their body weight and metabolic index during this period (*Figure 1A*). From the second week onward, mice in the HFD group showed a mild increase in body weight compared to the ND group. The difference increased over time until the eighth week when it was about 27% (ND *vs.* HFD: 30.48±1.19 *vs.* 38.93±0.51 g; *Figure 1B*), which was similar to the clinical mild obesity/overweight state. In the context of metabolism, the glucose level increased significantly in the HFD group after 4 weeks of feeding and became more obvious at 8 weeks (*Figure 1C*). After 8 weeks of feeding, serum insulin increased obviously, as blood glucose levels increased in HFD mice compared with ND mice (*Figure 1D*). Levels of serum TG, CH, and LDL-C increased following 8-week HFD feeding (*Figure 1D*). These results showed that 8-week HFD feeding established experimental models with mild obesity or that were overweight, consistent with the previous study (10). To further investigate whether 8-week HFD affects cardiac function and structure, mice were examined by echocardiography after an 8-week food intervention (*Figure 1A*). Measurements of LVEF, FS, LVESV, and LVEDV were comparable in ND and HFD mice (Figure S1 and Table S1), showing that a short-term HFD did not cause significant alteration in cardiac systolic function and structure. In other words, unlike a long-term HFD that could give rise to cardiac remodeling (11), 8-week HFD in this study did not result in cardiac dysfunction.

To explore the effect of 12-week HFD on left ventricular (LV) remodeling post-MI, we performed permanent coronary ligation surgery on mice after 8-week ND or HFD feeding. After MI surgery, mice were kept on the same diet as before surgery. We examined the subsequent cardiac functional alterations by echocardiography 7 and 28 days later (*Figure 1A*). Mice subjected to the HFD developed less pronounced ventricular remodeling and systolic dysfunction as indicated by higher LVEF and FS and lower LVESV and LVEDV at 7 and 28 days post-MI (*Figure 1E,1F* and Table S2). Masson's trichrome staining showed less fibrosis in the hearts of HFD mice than in those of ND mice (*Figure 1G*). These results consistently indicated that 12-week HFD feeding alleviated LV remodeling and improved cardiac function post-MI.

### *Twelve-week HFD attenuated local cardiac inflammation*

The vital role of excessive inflammation in ventricular remodeling post-MI is well documented (6). Thus, considering the close correlation between obesity and inflammation, we inferred that the 12-week impact of HFD on LV remodeling might be a negative regulator of inflammation after MI. We evaluated the infiltration of immune cell populations using flow cytometry. The number of total $CD45^+$ leukocytes that infiltrated in the heart was significantly lower in HFD mice than in ND mice at 7 days after MI (*Figure 2A*). However, the total number of leukocytes in the spleen and mediastinal lymph nodes (mLNs) was comparable in the two groups (Figure S2A,S2B). With further analysis of the leukocyte subsets, we found that $Ly6G^+$ neutrophils decreased in frequency and absolute numbers in HFD mice compared to their counterparts both in the heart and spleen (*Figure 2B,2C*); meanwhile, neutrophil counts were comparable in the mLNs (Figure S2C). Additionally, 12-week HFD dramatically reduced $CD3^-$ $CD64^+$ macrophages in frequency and absolute number in the heart (*Figure 2D* and Figure S3). Notably, the frequency of $CD206^-$ M1 macrophages diminished, while the frequency of $CD206^+$ M2 increased in HFD mice (*Figure 2D* and Figure S3) (12). This demonstrated an anti-inflammatory macrophages phenotype marked by dominant M2 macrophage infiltration in the heart of HFD mice (*Figure 2E*). In accordance with the decreased number and proportion of M1 macrophages, the myocardial expression of *Il1b* and *Il6* mRNA as M1 markers significantly decreased by day 7 after MI upon 12-week HFD feeding (*Figure 2F*). Taken together, these data indicated a reduced deposit of total leukocytes and neutrophils and a higher proportion of anti-inflammatory M2 macrophages in the infarcted heart, suggesting a reduction of cardiac local inflammation post-MI upon 12-week HFD.

### *Tregs were expanded after MI upon 12-week HFD*

Tregs, known for their powerful regulatory function in immune response, are essential for alleviating excessive inflammation and are helpful in improving ventricular remodeling post-MI. To define whether decreased myocardial inflammation caused by 12-week HFD was associated with Tregs, we evaluated the Tregs infiltration in the heart, spleen, and mLNs 7 days after MI. The number of Tregs infiltrated in the infarcted hearts of HFD

 

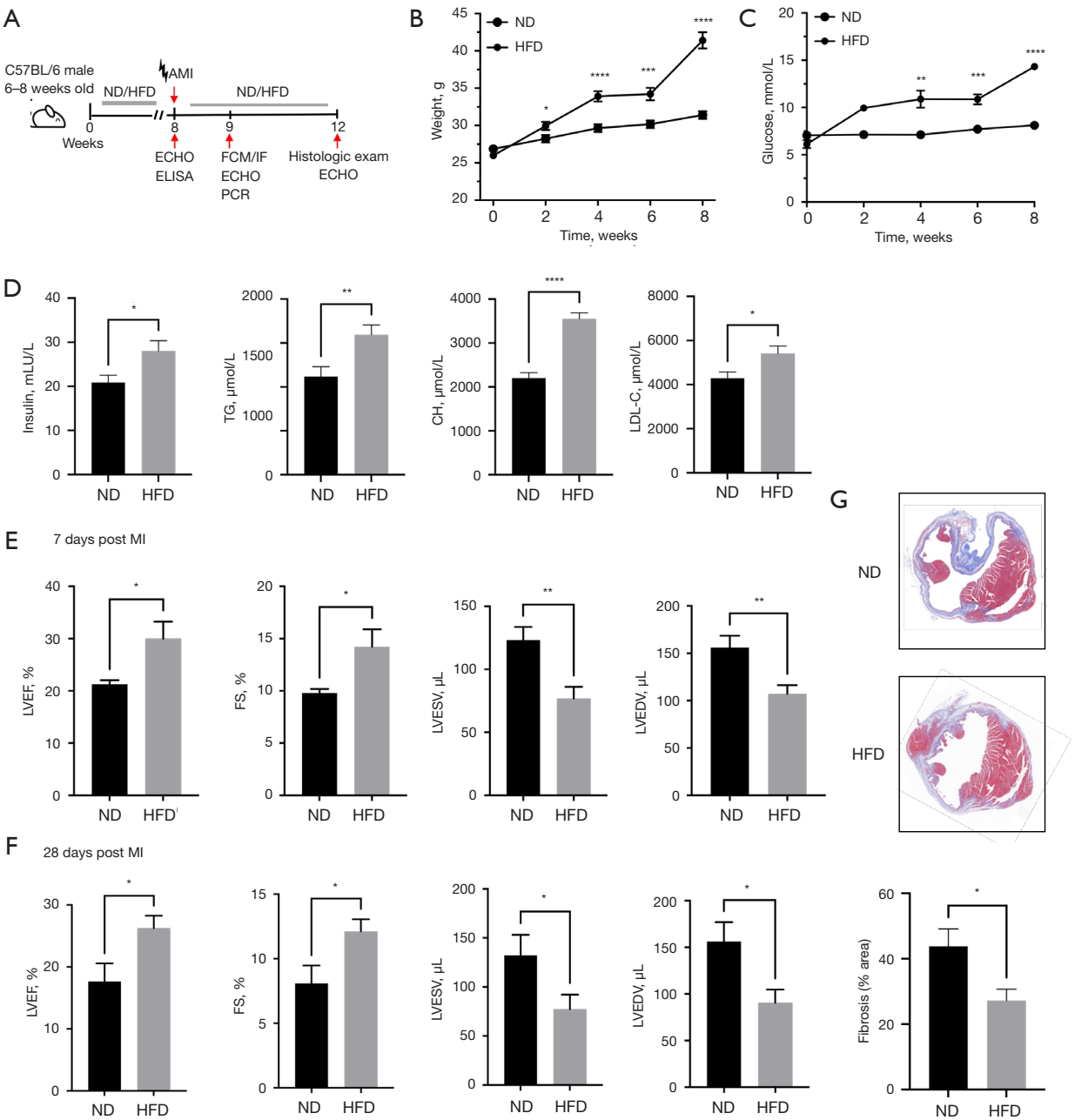


**Figure 1** Twelve-week HFD improved cardiac function and reduced ventricular remodeling after MI. (A) Experimental schematic. Six to 8-week-old male mice were fed ND or HFD for 8 weeks before receiving permanent coronary ligation surgery, and parameters were measured on designated days. (B,C) Body weight (B) and glucose level (C) of mice during 8-week ND or HFD feeding at the indicated time points. (D) Levels of serum insulin, TG, CH, and LDL-C after 8-week ND or HFD feeding. (E,F) Group data for LVEF, FS, LVESV, and LVEDV from ND and HFD-treated mice 7 (E) and 28 (F) days after MI. (G) Representative Masson trichrome staining of cardiac tissue sections in ND- and HFD-treated mice 28 days after MI. Group quantitation of peri-infarct interstitial fibrosis (% area) in mice hearts treated with ND or HFD. Scale bar, 1,000 μm. N=8 to 9/group. All error bars denote the mean ± SEM. *P<0.05; **P<0.01; ***P<0.001; ****P<0.0001. AMI, acute myocardial infarction; ND, normal diet; HFD, high-fat diet; ECHO, echocardiography; ELISA, enzyme-linked immunosorbent assay; FCM, flow cytometry; IF, immunofluorescence; PCR, polymerase chain reaction; TG, triglyceride; CH, total cholesterol; LDL-C, low-density lipoprotein cholesterol; MI, myocardial infarction; LVEF, left ventricular ejection fraction; FS, fractional shortening; LVESV, left ventricular end systolic volume; LVEDV, left ventricular end diastolic volume; SEM, standard error of mean.

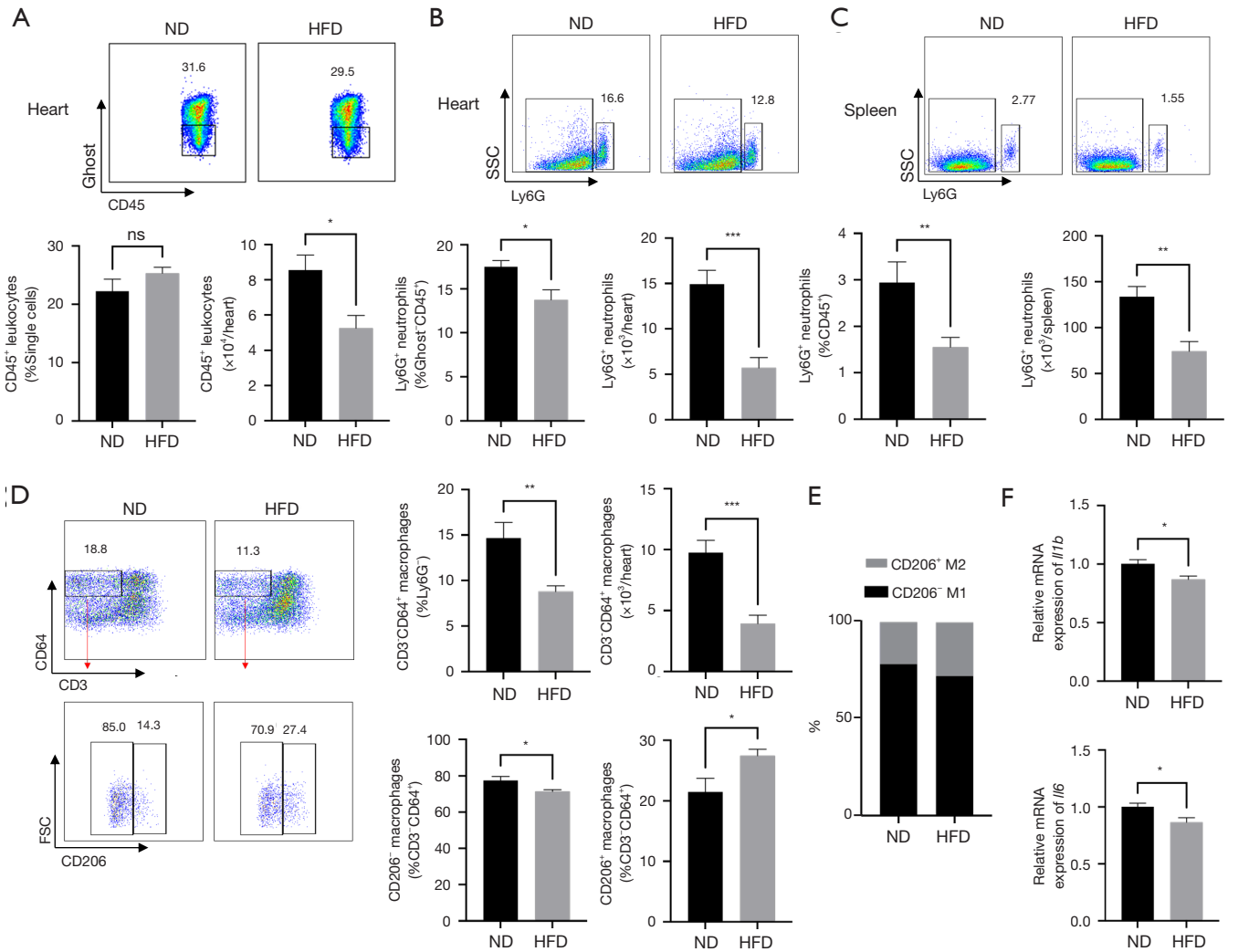


**Figure 2** Twelve-week HFD reduced local cardiac inflammation. (A) Representative flow cytometry scatter plots and quantitative data for CD45$^+$ leukocytes in the heart of ND- and HFD-treated mice 7 days after MI. (B,C) Representative flow cytometry scatter plots and quantitative data for Ly6G$^+$ neutrophils in the heart (B) and spleen (C) of ND- and HFD-treated mice 7 days after MI. (D) Representative flow cytometry scatter plots and quantitative data for CD3$^-$CD64$^+$ macrophages and its subsets CD206$^-$ M1 and CD206$^+$ M2 macrophages in the heart of ND- and HFD-treated mice 7 days after MI. (E) Proportion of M1 and M2 in the heart of ND- and HFD-treated mice 7 days after MI. (F) Expression levels of *Il1b* and *Il6* in the infarcted region 7 days after MI as determined by reverse-transcription quantitative polymerase chain reaction. N=6 to 7/group. All error bars denote the mean ± SEM. *P<0.05; **P<0.01; ***P<0.001; ns, not significant. ND, normal diet; HFD, high-fat diet; SSC, side scatter; FSC, forward scatter; MI, myocardial infarction; SEM, standard error of mean.

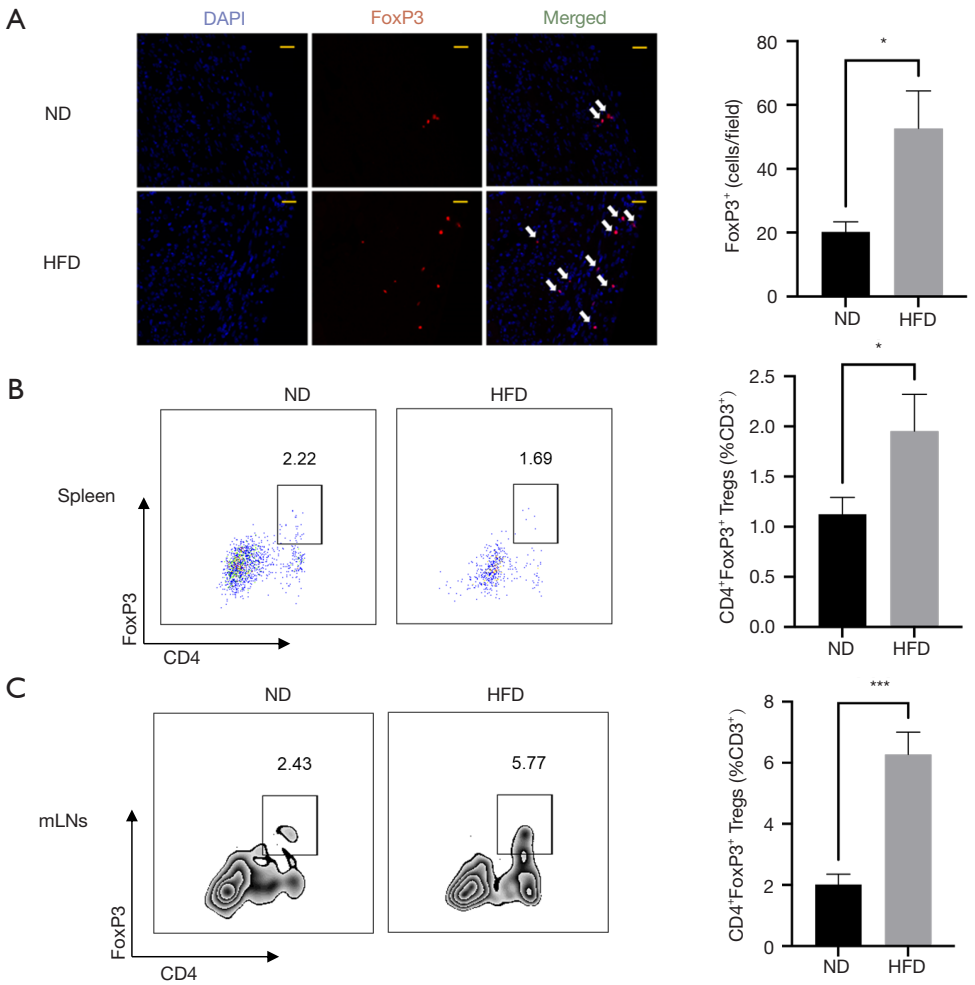


**Figure 3** Tregs expansion after MI upon 12-week HFD. (A) Representative immunofluorescence imaging of FoxP3$^+$ (red) in the heart of ND- and HFD-treated mice 7 days after MI and quantitation of FoxP3$^+$ cells. DAPI (blue) was used to label nuclei. The white arrow indicates FoxP3$^+$ cells. Scale bar, 20 μm. (B,C) Representative flow cytometry scatter plots and quantitative data for CD4$^+$FoxP3$^+$ Tregs in the spleen and mLNs of ND- and HFD-treated mice 7 days after MI. N=5 to 9/group. All error bars denote the mean ± SEM. *P<0.05; ***P<0.001. ND, normal diet; HFD, high-fat diet; DAPI, 4,6-diamidino-2-phenylindole; Treg, regulatory T cell; mLNs, mediastinal lymph nodes; MI, myocardial infarction; SEM, standard error of mean.

mice increased notably compared to those of ND mice (*Figure 3A*) even though the frequency and the absolute number of T cells remained the same between the two groups (Figure S4). Both in the spleen and mLNs, Tregs were markedly increased in HFD mice compared to ND mice (*Figure 3B,3C* and Figure S5). Altogether, these data verified that there was increased recruitment of Tregs into the myocardium and a higher level of Tregs in secondary lymph organs after MI upon 12-week HFD feeding.

### *Twelve-week HFD feeding impaired DCs function*

Since Tregs may modulate immune responses through DCs (8,9,13), we wondered whether an increased recruitment of Tregs in the myocardium induced by a 12-week HFD would be accompanied by changes in DCs. In this study, we examined the infiltration of DCs subsets, conventional DCs (cDCs), and monocyte-derived DCs (moDCs; *Figure 4A* and Figure S6). As shown in *Figure 4B*, compared with ND feeding, 12-week HFD decreased cDCs and

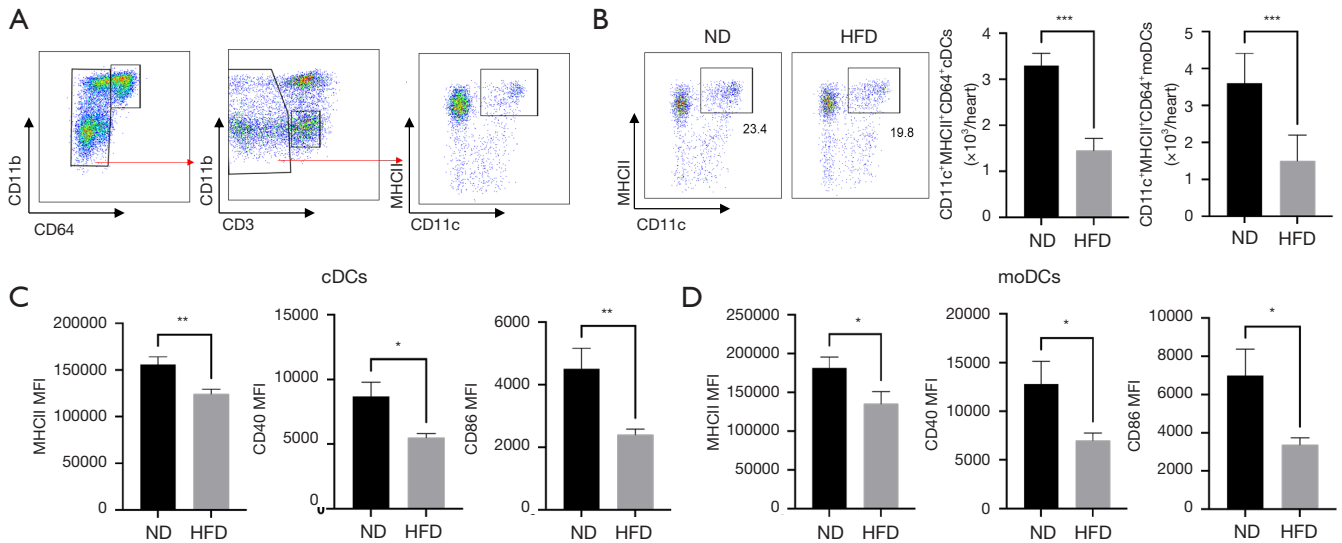


**Figure 4** Twelve-week HFD feeding impaired DCs function. (A) Flow cytometry scatter plots showing the gating for CD11c$^+$MHCII$^+$CD64$^-$ cDCs and CD11c$^+$MHCII$^+$CD64$^+$ moDCs among total CD45$^+$ leukocytes. (B) Quantification of cDCs and moDCs per heart of ND- and HFD-treated mice 7 days after MI. (C,D) MHCII, CD40, and CD86 MFI level in cDCs (C) and moDCs (D) of mLNs isolated from mice after ND and HFD feeding. N=6 to 8/group. All error bars denote the mean ± SEM. *P<0.05; **P<0.01; ***P<0.001. MHCII, major histocompatibility complex class II; ND, normal diet; HFD, high-fat diet; DCs, dendritic cells; cDCs, conventional DCs; moDCs, monocyte-derived DCs; MFI, mean fluorescence intensity; mLNs, mediastinal lymph nodes; MI, myocardial infarction; SEM, standard error of mean.

moDCs in the heart, indicating a striking reduction in recruitment of these two DCs types into the myocardium. There were no differences in the frequencies or absolute numbers of cDCs and moDCs in the heart-draining lymph, namely mLNs, between HFD mice and ND mice at 7 days post-MI. Importantly, we found that the MHCII mean fluorescent intensity (MFI) level of an individual cell in cDCs and moDCs in mLNs that was isolated from mice after HFD feeding decreased (*Figure 4C*,*4D*), indicating a lower maturation state and reduced capacity for antigen presentation. CD40 and CD86 are costimulatory factors related to the activation and maturation of DCs; their MFI levels in cDCs and moDCs decreased in the mLNs in the HFD group (*Figure 4C*,*4D*). Our findings of reduced MHCII, CD40, and CD86 MFI levels on cDCs and moDCs in the mLNs indicate that the reduced cardiac local inflammation upon HFD feeding may result from an impaired capacity of these DCs.

## Discussion

Our study generated several original findings. First, 8-week feeding with HFD caused metabolic alterations without affecting cardiac function and structure. Second, 8-week HFD feeding improved cardiac function and reduced ventricular remodeling at 7 and 28 days post-MI. Third, the protective effect of HFD on ventricular remodeling after MI was attributed to alleviated inflammation mediated by immune cells, featured by dramatically diminished proinflammatory neutrophils, a higher proportion of M2/M1 macrophages, augmented anti-inflammatory Tregs, and dysfunctional DCs. Taken together, these findings demonstrate that HFD feeding has an important role in ventricular remodeling post-MI, which is mediated by immune cell populations. These findings also suggest that using the HFD may be a fruitful approach to improving the prognosis of MI, providing new insight into the mechanism of the obesity paradox phenomenon.

We established experimental permanent MI models using permanent coronary ligation to clarify the impact of 12-week HFD on ventricular remodeling post-MI. To examine the clinical relationship between mild obesity or being overweight and the prognosis of MI patients, we applied an up to 12-week HFD intervention to induce mild obesity on the experimental permanent MI mice. There is no specific definition of “mild obesity” or “overweight”

 

status, but 12-week HFD has recently been demonstrated to increase weight range with reference to ND-fed mice. HFD-fed mice are commonly reported as being obese and to undergo metabolic changes, mimicking an overweight or mild obesity phenotype (10). We started to feed mice with HFD for 8 weeks before MI and continued after MI. The 8-week HFD-fed mice, compared to ND-fed mice, increased in body weight (20–40%) and had the metabolic profile of hyperglycemia, hyperinsulinemia, and hyperlipemia. Consistent with a previous report, these metabolic alterations caused by the 8-week HFD mirrored changes described in overweight individuals without reaching morbid obesity (10). Further, echocardiography verified that the 8-week HFD did not induce obvious alterations in cardiac general structure or function. Thus, our findings on this 8-week HFD-fed model are of reference significance for research on the mechanism underlying the better clinical outcomes of overweight/mild obese MI patients.

By establishing permanent MI in this HFD-fed model, we definitively observed that a 12-week HFD facilitated cardiac repair post-MI, reducing ventricular enlargement and fibrosis and improving cardiac function. This result from permanent MI models was consistent with previous works based on ischemia/reperfusion (I/R) injury models (14,15). Poncelas (14) showed that B6D2F1 mice that were fed with HFD for 6 months before and 1 month after MI I/R injury showed a marked reduction in infarct size (~50%) and cardiac dilation compared to controls. The HFD used in these studies was similar to ours with 60% kcal/fat, while the duration of HFD we used was well within that of these previous studies on HFD feeding and cardiac ischemic repair (10). Therefore, we have provided further evidence for the benefits of 12-week HFD to ventricular remodeling post-MI using MI models with permanent ligation.

Excessive inflammation is well documented to be attributed to ventricular remodeling (16). After MI, massive cell death triggers an intense inflammatory response for the removal of necrotic debris, and after 3–5 days, this process should be properly resolved, shifting into a relative anti-inflammatory phase that leads to tissue repair (6,16). We found a notable reduction of inflammation at 7 days post-MI in the 12-week HFD-fed group, marked by an apparent decrease of overall myocardial leukocytes. Among the decreased leukocytes, neutrophils, the first inflammatory cells to migrate into the myocardium as key effectors of the innate immune response, decrease systemically in mice with 12-week HFD feeding compared with ND mice (6,16). Although total depletion of neutrophils during the initial inflammatory response was reported to harm cardiac repair after MI, neutrophils were recognized as pathological cells resulting from ventricular remodeling (17). Evidence includes their tendency to degrade the extracellular matrix by releasing matrix metalloproteinases. Our findings indicated that 12-week HFD protects mice from excessive neutrophils infiltrating the heart and could ameliorate adverse ventricular remodeling.

Interestingly, in addition to a marked reduction of macrophage recruitment into the injury myocardium, we observed that macrophages that infiltrated the infarcted heart of HFD mice consisted of more anti-inflammatory M2 macrophages and less proinflammatory M1 macrophages in contrast to that of ND mice, accompanied by less *Il1b* and *Il6* in the injured heart. This result supports the presence of a local reparative environment in 12-week HFD mice, featured by predominant M2 macrophages that can resolve excessive inflammation in a timely manner and subsequently lessen post-MI remodeling. Our findings also shed light on Tregs, as it has been consistently documented that they can improve cardiac recovery after MI with their powerful immune regulatory function, for instance, by promoting macrophage polarization toward more anti-inflammatory M2 macrophages as the predominant phenotype (18,19). Notably, we observed increased recruitment of Tregs into the myocardium and a higher level of Tregs in secondary lymph organs in the 12-week HFD-fed mice. The improved cardiac function and reduction of local proinflammatory immune cells of the heart after MI may be due to the extensive expansion of Tregs.

Prior work has shown that restriction of DCs-mediated immunity is beneficial to ventricular remodeling after MI (20,21). Moreover, Tregs are known to suppress inflammation by downregulating the costimulatory molecules CD80 and CD86 of DCs (8,9,13). This may be an additional effector function of Tregs (8,9,13). We also observed reduced recruitment of moDCs and cDCs into the infarcted myocardium. The maturation and antigen-presenting capacity of DCs are related to the high surface expression of MHCII and costimulatory molecules, which are essential for DCs-dependent T cell activation (22). Of note, the expressions of MHCII and costimulatory molecules CD40 and CD86 on cDCs and moDCs in mLNs were downregulated after MI in the background of

 

12-week HFD feeding. Our findings suggest that the reduction of cDCs and moDCs in the heart and their dysfunction in mLNs may partly contribute to the changes of macrophages caused by Tregs upon 12-week HFD feeding as indicated by the downregulation of MHCII and costimulatory molecules.

However, the mechanism by which HFD may alleviate ventricular remodeling by reducing cardiac inflammation remains unknown. Related studies suggest that some adipokines secreted by adipose tissue might attenuate inflammatory responses (23,24). Interleukin-33 (IL-33) levels are directly correlated with leptin levels in mice and men (25), and HFD mice have higher leptin and IL-33 levels than their lean littermates (26,27). Meanwhile, Tregs accumulate in infarcted myocardium to exert protective effects through the IL-33/ST2 axis (7). Therefore, the level of IL-33 would be higher in the HFD group, and IL-33 would have expanded Tregs through the IL-33/ST2 signaling pathway. Furthermore, a HFD could activate cyclic GMP-AMP synthase (cGAS)/stimulator of interferon genes (STING) signaling, nuclear factor kappa-B (NF-κB) signaling (28,29), and Toll-like receptors (TLRs) (2/3/4) signaling (30). cGAS, as the primary cytosolic DNA sensor, recognizes various pathogen-associated molecular patterns to initiate and enhance inflammation (31). Research shows that cGAS/STING (32) and TLRs (33) promote NF-κB activation. The transcription factor NF-κB is crucial for the expression of FoxP3 and the development of Tregs (34). Therefore, HFD may activate cGAS/STING signaling or TLRs signaling to enhance the expression of FoxP3. In addition, increased fatty acid oxidation and CD36 in HFD recipients may stabilize Foxp3 expression (35,36), thereby modulating Tregs differentiation, stabilization, and function (36).

### *Strengths and limitations*

This study is the first of its kind to establish experimental permanent MI models using permanent coronary ligation to clarify the impact of 12-week HFD on ventricular remodeling post-MI. Furthermore, we found immune cells may account for the beneficial impact of 12-week HFD and were associated with various changes in inflammatory cells.

This study had some limitations. First, even though we found several changes in immune cells after 12-week HFD, such as the anti-inflammatory phenotype of macrophages, Tregs expansion, and DCs reduction and dysfunction, further efforts are needed to verify the causal relationship between these alterations and the improved adverse remodeling. Second, the immune profile in the blood could reflect systemic inflammation. The immune cells mainly interact via the cytokine-chemokine network. Chemokines and cytokines play crucial roles in cardiac inflammation by directing the trafficking of infiltrating immune cells and their interactions (37). These parameters should be taken into account in our future research. Third, we suggest future studies should be conducted to assess changes in immune systems in overweight or mild obesity patients to further clarify the protective clues for MI patients' cardiac repair. Fourth, whether other immune or nonimmune cells also contribute to the benefits of 12-week HFD is unclear because we focused only on the predominant and well-documented significance of certain cells (e.g., macrophages and Tregs) in cardiac inflammation after MI. Fifth, a sham control group should have been included in the study, given that the surgery for MI can cause a severe inflammatory response. Sixth, many studies have reported that high-fat feeding results in increased blood pressure (38) and that hypertension affects cardiac remodeling and fibrosis (39,40). However, our study did not clarify the relationship among blood pressure, cardiac fibrosis, and the HFD.

## Conclusions

We demonstrated that a 12-week HFD can alleviate inflammation following MI and consequently improve adverse ventricular remodeling post-acute MI. Our results strongly suggest that 12-week HFD can promote macrophage polarization into a repair-favoring phenotype. This might be a consequence of increased Tregs infiltration in the infarcted myocardium and the dysfunction of cDCs and moDCs (*Figure 5*).

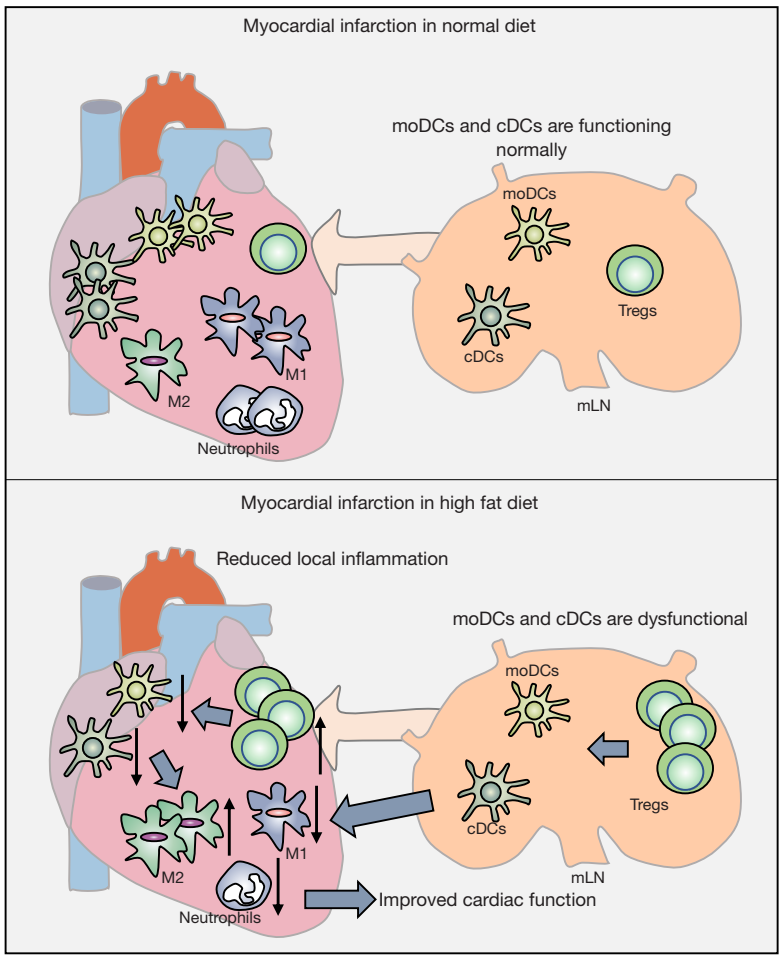


**Figure 5** Schematic overview of how the 12-week HFD improved adverse ventricular remodeling post-MI by alleviating local inflammation. Twelve-week HFD promoted reduced infiltration of neutrophils and macrophage polarization into a repair-favoring phenotype. This might be a consequence of increased Tregs infiltration in the infarcted myocardium, potentially via dysfunction of the cDCs and moDCs. DCs, dendritic cells; moDCs, monocyte-derived DCs; cDCs, conventional DCs; M1, type 1 macrophages; M2, type 2 macrophages; Tregs, regulatory T cells; mLN, mediastinal lymph node; HFD, high-fat diet; MI, myocardial infarction.

## Acknowledgments

We thank the members of the Keli Yang Laboratory at Sun Yat-sen University for their research support.
*Funding:* This work was supported by the National Natural Science Foundation of China (No. 82070412 to SX and No. 81600238 to YC).

## Footnote

*Reporting Checklist:* The authors have completed the ARRIVE reporting checklist. Available at https://atm.amegroups.com/article/view/10.21037/atm-22-1218/rc

*Data Sharing Statement:* Available at https://atm.amegroups.com/article/view/10.21037/atm-22-1218/dss

*Peer Review File:* Available at https://atm.amegroups.com/article/view/10.21037/atm-22-1218/prf

*Conflicts of Interest:* All authors have completed the ICMJE uniform disclosure form (available at https://atm.amegroups.com/article/view/10.21037/atm-22-1218/coif). The authors have no conflicts of interest to declare.

*Ethical Statement:* The authors are accountable for all

aspects of the work in ensuring that questions related to the accuracy or integrity of any part of the work are appropriately investigated and resolved. Experiments were performed under a project license (license no. of laboratory animal facility: SYXK [Guangdong] 2019-0209) granted by the ethics committee of Sun Yat-sen University and in compliance with the Institutional Animal Care and Use Committee (IACUC; Eighth Edition) for the care and use of animals.



## References

1. Roger VL. Epidemiology of heart failure. Circ Res 2013;113:646-59.
2. Cahill TJ, Kharbanda RK. Heart failure after myocardial infarction in the era of primary percutaneous coronary intervention: Mechanisms, incidence and identification of patients at risk. World J Cardiol 2017;9:407-15.
3. Lopez-Jaramillo P, Joseph P, Lopez-Lopez JP, et al. Risk factors, cardiovascular disease, and mortality in South America: a PURE substudy. Eur Heart J 2022;43:2841-51.
4. Rodríguez-Castro E, Rodríguez-Yáñez M, Arias-Rivas S, et al. Obesity Paradox in Ischemic Stroke: Clinical and Molecular Insights. Transl Stroke Res 2019;10:639-49.
5. Wang L, Liu W, He X, et al. Association of overweight and obesity with patient mortality after acute myocardial infarction: a meta-analysis of prospective studies. Int J Obes (Lond) 2016;40:220-8.
6. Ong SB, Hernández-Reséndiz S, Crespo-Avilan GE, et al. Inflammation following acute myocardial infarction: Multiple players, dynamic roles, and novel therapeutic opportunities. Pharmacol Ther 2018;186:73-87.
7. Xia N, Lu Y, Gu M, et al. A Unique Population of Regulatory T Cells in Heart Potentiates Cardiac Protection From Myocardial Infarction. Circulation 2020;142:1956-73.
8. Cederbom L, Hall H, Ivars F. CD4+CD25+ regulatory T cells down-regulate co-stimulatory molecules on antigen-presenting cells. Eur J Immunol 2000;30:1538-43.
9. Misra N, Bayry J, Lacroix-Desmazes S, et al. Cutting edge: human CD4+CD25+ T cells restrain the maturation and antigen-presenting function of dendritic cells. J Immunol 2004;172:4676-80.
10. Schröder T, Wiese AV, Ender F, et al. Short-term high-fat diet feeding protects from the development of experimental allergic asthma in mice. Clin Exp Allergy 2019;49:1245-57.
11. Wang Z, Li L, Zhao H, et al. Chronic high fat diet induces cardiac hypertrophy and fibrosis in mice. Metabolism 2015;64:917-25.
12. Yan X, Anzai A, Katsumata Y, et al. Temporal dynamics of cardiac immune cell accumulation following acute myocardial infarction. J Mol Cell Cardiol 2013;62:24-35.
13. Tang Q, Adams JY, Tooley AJ, et al. Visualizing regulatory T cell control of autoimmune responses in nonobese diabetic mice. Nat Immunol 2006;7:83-92.
14. Poncelas M, Inserte J, Vilardosa Ú, et al. Obesity induced by high fat diet attenuates postinfarct myocardial remodeling and dysfunction in adult B6D2F1 mice. J Mol Cell Cardiol 2015;84:154-61.
15. Haar L, Ren X, Liu Y, et al. Acute consumption of a high-fat diet prior to ischemia-reperfusion results in cardioprotection through NF-κB-dependent regulation of autophagic pathways. Am J Physiol Heart Circ Physiol 2014;307:H1705-13.
16. Westman PC, Lipinski MJ, Luger D, et al. Inflammation as a Driver of Adverse Left Ventricular Remodeling After Acute Myocardial Infarction. J Am Coll Cardiol 2016;67:2050-60.
17. Hofmann U, Frantz S. Role of lymphocytes in myocardial injury, healing, and remodeling after myocardial infarction. Circ Res 2015;116:354-67.
18. Tang TT, Yuan J, Zhu ZF, et al. Regulatory T cells ameliorate cardiac remodeling after myocardial infarction. Basic Res Cardiol 2012;107:232.
19. Weirather J, Hofmann UD, Beyersdorf N, et al. Foxp3+ CD4+ T cells improve healing after myocardial infarction by modulating monocyte/macrophage differentiation. Circ Res 2014;115:55-67.
20. Lee JS, Jeong SJ, Kim S, et al. Conventional Dendritic Cells Impair Recovery after Myocardial Infarction. J Immunol 2018;201:1784-98.
21. Maekawa Y, Mizue N, Chan A, et al. Survival and cardiac remodeling after myocardial infarction are critically dependent on the host innate immune interleukin-1 receptor-associated kinase-4 signaling: a regulator

 

of bone marrow-derived dendritic cells. Circulation 2009;120:1401-14.
22. Ma DY, Clark EA. The role of CD40 and CD154/CD40L in dendritic cells. Semin Immunol 2009;21:265-72.
23. Wolk R, Bertolet M, Singh P, et al. Prognostic Value of Adipokines in Predicting Cardiovascular Outcome: Explaining the Obesity Paradox. Mayo Clin Proc 2016;91:858-66.
24. Rauchhaus M, Coats AJ, Anker SD. The endotoxin-lipoprotein hypothesis. Lancet 2000;356:930-3.
25. Zeyda M, Wernly B, Demyanets S, et al. Severe obesity increases adipose tissue expression of interleukin-33 and its receptor ST2, both predominantly detectable in endothelial cells of human adipose tissue. Int J Obes (Lond) 2013;37:658-65.
26. Cichon I, Ortmann W, Santocki M, et al. Scrutinizing Mechanisms of the 'Obesity Paradox in Sepsis': Obesity Is Accompanied by Diminished Formation of Neutrophil Extracellular Traps (NETs) Due to Restricted Neutrophil-Platelet Interactions. Cells 2021;10:384.
27. Zhao XY, Zhou L, Chen Z, et al. The obesity-induced adipokine sST2 exacerbates adipose Treg and ILC2 depletion and promotes insulin resistance. Sci Adv 2020;6:eaay6191.
28. Gong Y, Li G, Tao J, et al. Double knockout of Akt2 and AMPK accentuates high fat diet-induced cardiac anomalies through a cGAS-STING-mediated mechanism. Biochim Biophys Acta Mol Basis Dis 2020;1866:165855.
29. Vykhovanets EV, Shankar E, Vykhovanets OV, et al. High-fat diet increases NF-κB signaling in the prostate of reporter mice. Prostate 2011;71:147-56.
30. Zhang G, Li R, Li W, et al. Toll-like receptor 3 ablation prevented high-fat diet-induced obesity and metabolic disorder. J Nutr Biochem 2021;95:108761.
31. Kawai T, Akira S. The roles of TLRs, RLRs and NLRs in pathogen recognition. Int Immunol 2009;21:317-37.
32. Balka KR, Louis C, Saunders TL, et al. TBK1 and IKKε Act Redundantly to Mediate STING-Induced NF-κB Responses in Myeloid Cells. Cell Rep 2020;31:107492.
33. Wypasek E, Natorska J, Mazur AI, et al. Toll-like receptors expression and NF-κB activation in peritoneal leukocytes in morphine-mediated impairment of zymosan-induced peritonitis in swiss mice. Arch Immunol Ther Exp (Warsz) 2012;60:373-82.
34. Long M, Park SG, Strickland I, et al. Nuclear factor-kappaB modulates regulatory T cell development by directly regulating expression of Foxp3 transcription factor. Immunity 2009;31:921-31.
35. Inserte J, Aluja D, Barba I, et al. High-fat diet improves tolerance to myocardial ischemia by delaying normalization of intracellular PH at reperfusion. J Mol Cell Cardiol 2019;133:164-73.
36. Shi H, Chi H. Metabolic Control of Treg Cell Stability, Plasticity, and Tissue-Specific Heterogeneity. Front Immunol 2019;10:2716.
37. Hanna A, Frangogiannis NG. Inflammatory Cytokines and Chemokines as Therapeutic Targets in Heart Failure. Cardiovasc Drugs Ther 2020;34:849-63.
38. Noh MR, Kong MJ, Han SJ, et al. Isocitrate dehydrogenase 2 deficiency aggravates prolonged high-fat diet intake-induced hypertension. Redox Biol 2020;34:101548.
39. Mouton AJ, Flynn ER, Moak SP, et al. Interaction of Obesity and Hypertension on Cardiac Metabolic Remodeling and Survival Following Myocardial Infarction. J Am Heart Assoc 2021;10:e018212.
40. Watanabe S, Kumazaki S, Kusunoki K, et al. A High-Fat and High-Cholesterol Diet Induces Cardiac Fibrosis, Vascular Endothelial, and Left Ventricular Diastolic Dysfunction in SHRSP5/Dmcr Rats. J Atheroscler Thromb 2018;25:439-53.

**Cite this article as:** Yang J, Mai B, Su Y, Liang S, Su Z, Chen Y, Xie S. Twelve-week high-fat diet for improving adverse ventricular remodeling post-myocardial infarction by alleviating local inflammation. Ann Transl Med 2022;10(20):1089. doi: 10.21037/atm-22-1218

 

## Supplementary

**Table S1** qPCR forward and reverse primer sequences

| Gene name | Sequence |
|---|---|
| *Il1b* | Forward: CAACCAACAAGTGATATTCTCCATG |
| | Reverse: GATCCACACTCTCCAGCTGCA |
| *Il6* | Forward: GAGGATACCACTCCCAACAGACC |
| | Reverse: AAGTGCATCATCGTTGTTCATACA |

qPCR, quantitative polymerase chain reaction.

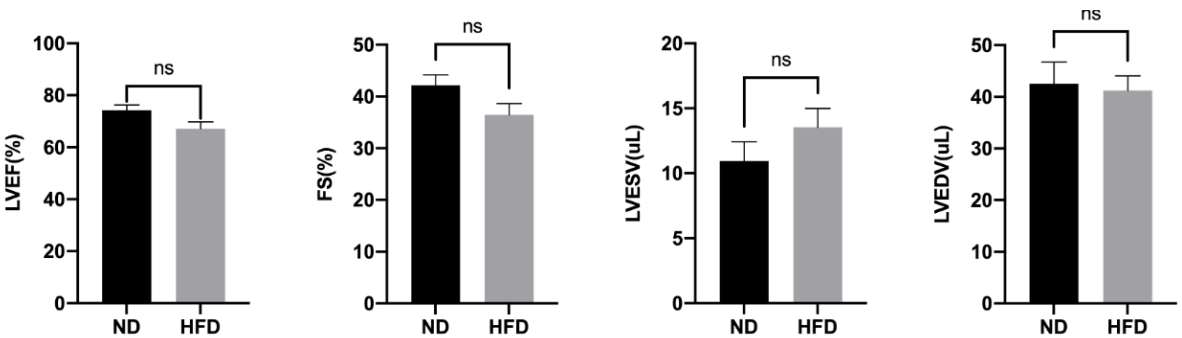


**Figure S1** Eight-week HFD feeding did not affect cardiac function and structure. Group data for LVEF, FS, LVESV and LVEDV from mice after 8-week ND or HFD feeding. Unpaired *t*-test. N=8 to 9/group. All error bars denote the mean ± SEM. ns, not significant. ND, normal diet; HFD, high-fat diet; LVEF, left ventricular ejection fraction; FS, fractional shortening; LVESV, left ventricular end systolic volume; LVEDV, left ventricular end diastolic volume; SEM, standard error of mean.


https://dx.doi.org/10.21037/atm-22-1218

**Table S2** Echocardiography characterization of ND and HFD mice

| Parameters | ND | | | HFD | | |
|---|---|---|---|---|---|---|
| | Before MI | 7 days MI | 28 days MI | Before MI | 7 days MI | 28 days MI |
| LVEF (%) | 74.24±2.072 | 21.22±0.7953 | 17.65±2.920 | 67.11±2.705 | 29.99±3.260* | 26.26±1.998* |
| FS (%) | 42.19±1.978 | 9.801±0.3810 | 8.097±1.380 | 36.49±2.172 | 14.21±1.676* | 12.12±0.9385* |
| LVESV (μL) | 10.94±1.483 | 123.2±10.55 | 132.4±20.82 | 13.54±1.443 | 76.81±9.347** | 77.45±14.88* |
| LVEDV (μL) | 42.53±4.202 | 156.0±12.52 | 156.4±20.62 | 41.24±2.835 | 107.2±9.300** | 90.63±14.17* |

Echocardiography was performed on the mice before MI and at the indicated time after MI. Unpaired *t*-test compared to ND. Values are means ± SEM. *P<0.05; **P<0.01. ND, normal diet; HFD, high-fat diet; LVEF, left ventricular ejection fraction; FS, fractional shortening; LVESV, left ventricular end systolic volume; LVEDV, left ventricular end diastolic volume; MI, myocardial infarction; SEM, standard error of mean.

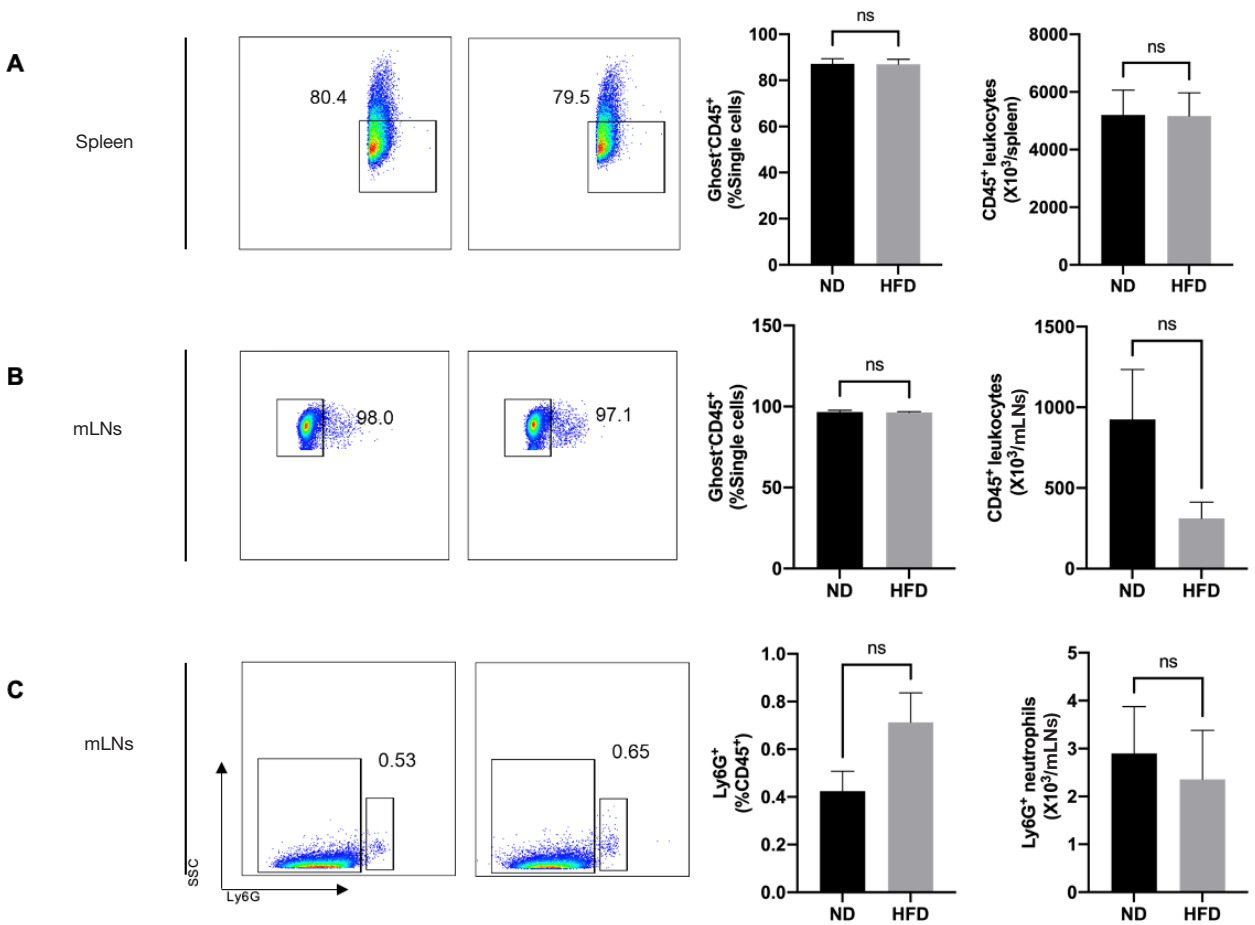


**Figure S2** Twelve-week HFD did not change leukocytes and neutrophils number in spleen and mLNs. (A,B) Representative flow cytometry scatter plots and quantitative data for $CD45^+$ leukocytes in the spleen (A) and mLNs (B) of ND and HFD-treated mice 7 days after MI. (C) Representative flow cytometry scatter plots and quantitative data for $Ly6G^+$ neutrophils in the mLNs of ND and HFD-treated mice 7 days after MI. N=8 to 9/group. All error bars denote the mean ± SEM. ns, not significant. ND, normal diet; HFD, high-fat diet; mLNs, mediastinal lymph nodes; SSC, side scatter; MI, myocardial infarction; SEM, standard error of mean.


https://dx.doi.org/10.21037/atm-22-1218

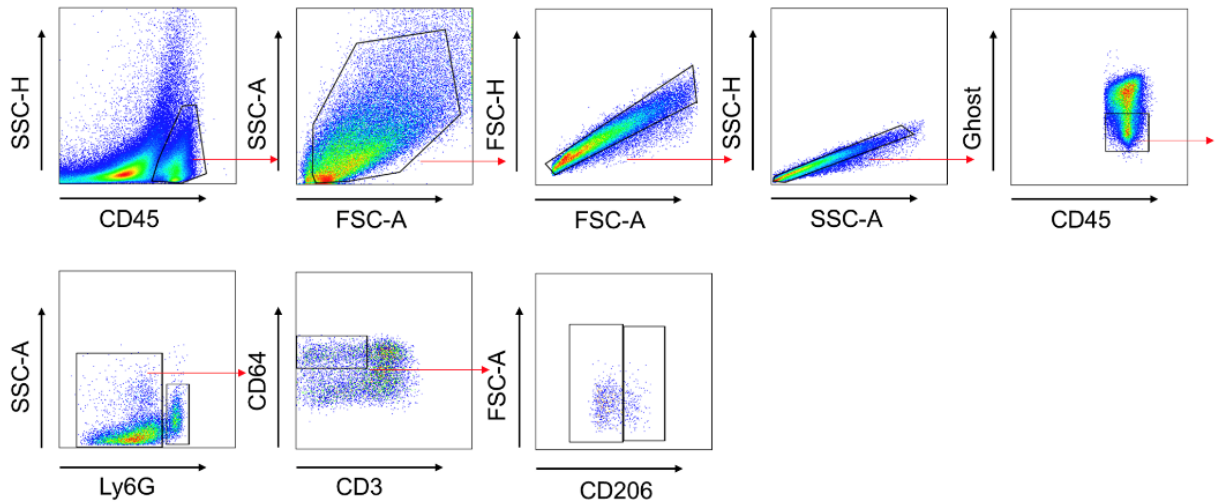


**Figure S3** TGating strategy of flow cytometry for macrophages. Flow cytometry scatter plots showing the gating for $CD45^{+}CD3^{-}Ly6G^{-}CD64^{+}$ macrophages. SSC, side scatter; FSC, forward scatter; H, height; A, area.

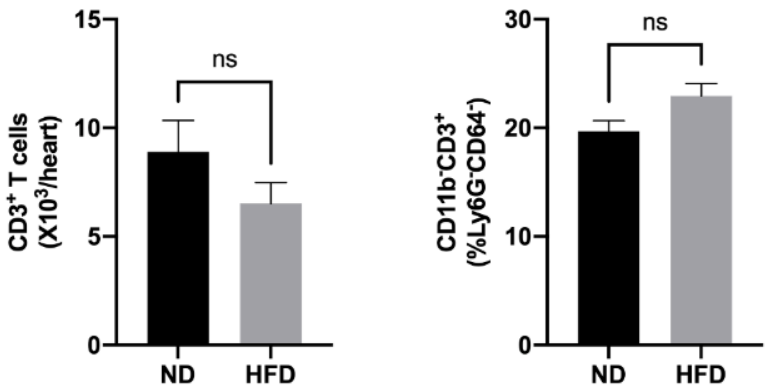


**Figure S4** Twelve-week HFD did not change T cells number in the heart. Quantitative data for $CD3^{+}$ T cells in the heart of ND and HFD-treated mice 7 days after MI. N=6 to 7/group. All error bars denote the mean ± SEM. ns, not significant. ND, normal diet; HFD, high-fat diet; MI, myocardial infarction; SEM, standard error of mean.


https://dx.doi.org/10.21037/atm-22-1218

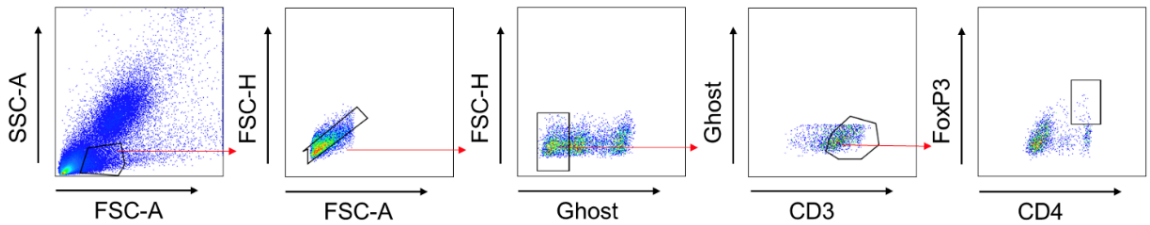


**Figure S5** Gating strategy of flow cytometry for Tregs. Flow cytometry scatter plots showing the gating for $CD3^{+}FoxP3^{+}$ Tregs. SSC, side scatter; FSC, forward scatter; H, height; A, area; Tregs, regulatory T cells.

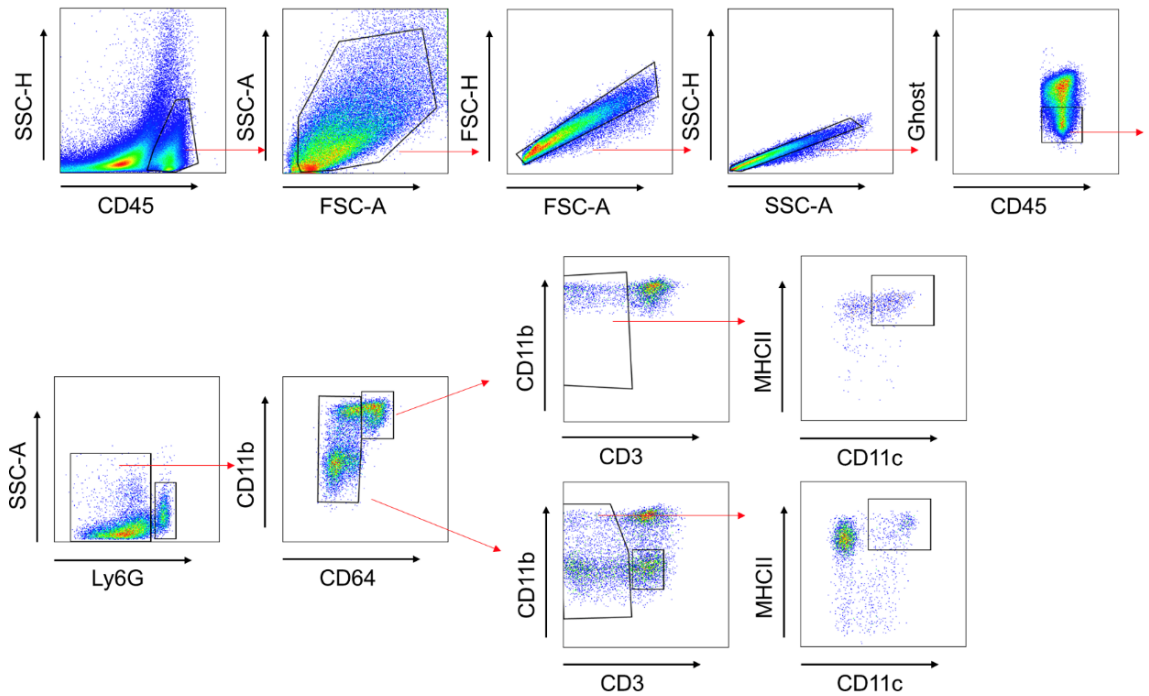


**Figure S6** Gating strategy of flow cytometry for cDCs and moDCs. Flow cytometry scatter plots showing the gating for $CD45^{+}CD3^{-}Ly6G^{-}CD11b^{+}MHCII^{+}CD64^{-}$ cDCs and $CD45^{+}CD3^{-}Ly6G^{-}CD11c^{+}MHCII^{+}CD64^{+}$ moDCs (C). SSC, side scatter; FSC, forward scatter; H, height; A, area; MHCII, major histocompatibility complex class II; DCs, dendritic cells; cDCs, conventional DCs; moDCs, monocyte-derived DCs.


https://dx.doi.org/10.21037/atm-22-1218